

Geometrical Optics in Coincidence Imaging System

De-Zhong Cao¹, Jun Xiong¹, and Kaige Wang^{2,1*}

1. *Department of Physics, Applied Optics Beijing Area Major Laboratory,
Beijing Normal University, Beijing 100875, China*

2. *CCAST (World Laboratory), P. O. Box 8730, Beijing 100080, China*

We discuss the geometrical optics of coincidence imaging for two kinds of spatial correlations which are related to a classical thermal light source and a two-photon quantum entangled state.

PACS number(s): 42.50.Dv, 42.30.Va, 42.65.Lm

A novel imaging method, called coincidence imaging (or ghost imaging), has drawn much attention recently [1]- [8]. In this imaging system, object and image are separately illuminated by a pair of correlated beams, and the image emerges with a coincidence detection of the two beams. The first coincidence imaging experiments were carried out by a pair of entangled photons generated in spontaneous parametric down-conversion (SPDC) [1] [2]. The effect can persist in a high gain of SPDC, in which two entangled beams contain a large number of photons [5]. Recently, the experiments have shown that the coincidence imaging can be emulated by classically correlated beams generated by randomly shooting of rays [6]. Theoretical studies have shown that a thermal source may possess the similar spatial correlation as that of entangled photon pair [3]- [5], [8]- [10]. Therefore, the effects related to two-photon entanglement, such as coincidence imaging, coincidence interference and subwavelength lithography, may have classical counterparts.

In this paper, we focus on the study in the macroscopic aspect of coincidence imaging: the geometrical optics. We find that the coincidence imaging exhibits distinct aspect which cannot be included in ordinary imaging. However, the difference of spatial correlation between quantum and classical sources is also reflected in the geometrical optics. In the SPDC of a type-I crystal, the down-converted beams contain both quantum entanglement and classical thermal correlation. When the crystal is used as a source, it can form a special dual coincidence imaging system, in which an object can simultaneously produce two coincidence images. The system may find potential application in new optical design.

We consider classical thermal light described by $E(\mathbf{x}, z, t) = \int E(\mathbf{q}) \exp[i\mathbf{q} \cdot \mathbf{x}] d\mathbf{q} \cdot \exp[i(kz - \omega t)]$, in which $E(\mathbf{q})$ is a stochastic variable obeying Gaussian statistics and \mathbf{q} is the transverse wavevector satisfying $|\mathbf{q}| \ll k$. For any thermal statistics, the second-order spectral correlation is written as

$$\begin{aligned} & \langle E^*(\mathbf{q}_1)E^*(\mathbf{q}_2)E(\mathbf{q}'_2)E(\mathbf{q}'_1) \rangle \\ &= \langle E^*(\mathbf{q}_1)E(\mathbf{q}'_1) \rangle \langle E^*(\mathbf{q}_2)E(\mathbf{q}'_2) \rangle + \langle E^*(\mathbf{q}_1)E(\mathbf{q}'_2) \rangle \langle E^*(\mathbf{q}_2)E(\mathbf{q}'_1) \rangle \\ &= S(\mathbf{q}_1)S(\mathbf{q}_2)[\delta(\mathbf{q}_1 - \mathbf{q}'_1)\delta(\mathbf{q}_2 - \mathbf{q}'_2) + \delta(\mathbf{q}_1 - \mathbf{q}'_2)\delta(\mathbf{q}_2 - \mathbf{q}'_1)], \end{aligned} \quad (1)$$

where $S(\mathbf{q})$ is the power spectrum of the spatial frequency. For comparison, we show the second-order correlation of the entangled beams generated in the lower gain limit of SPDC

$$\langle a_m^\dagger(\mathbf{q}_1)a_n^\dagger(\mathbf{q}_2)a_n(\mathbf{q}'_2)a_m(\mathbf{q}'_1) \rangle = W^*(\mathbf{q}_1)W(\mathbf{q}'_1)\delta(\mathbf{q}_1 + \mathbf{q}_2)\delta(\mathbf{q}'_1 + \mathbf{q}'_2). \quad (2)$$

where the subscripts m and n indicate the polarizations of the beams for a type II crystal. The spectrum $W(\mathbf{q})$ depends on the transfer functions of SPDC [10]. The equation is also valid for a type I crystal, in which the down-converted beams have the same polarization, and the subscripts m and n can be omitted. Therefore, both the thermal light and the entangled photon pair exist the transverse wavevector correlation. The former shows the self-correlation of transverse wavevectors between positive and negative components, while the latter shows the correlation of a pair of conjugate wavevectors satisfying the momentum conservation, within the same component of spatial frequency.

To show coincidence imaging of thermal light, we may use a 50/50 beamsplitter which divides input beam into two correlated beams. On the other hand, in the collinear case of SPDC, the beamsplitter is also needed to spatially separate the entangled down-converted beams. We define $F_i(\mathbf{q})$ ($i = 1, 2$) as the two output fields of the beamsplitter. For both classical and quantum sources, the second-order correlation of the output fields $\langle F_1^*(\mathbf{q}_1)F_1(\mathbf{q}'_1)F_2^*(\mathbf{q}_2)F_2(\mathbf{q}'_2) \rangle$ is proportional to that of the input, i.e. Eqs. (1) and (2). For simplicity, we consider one dimension case. Let $h_i(x, x')$ ($i = 1, 2$) be the impulse response function for the i -path in the coincidence imaging scheme, the joint-intensity at the two detective planes is obtained to be

$$\langle I_1(x_1)I_2(x_2) \rangle = \int h_1^*(x_1, -q_1)h_1(x_1, -q'_1)h_2^*(x_2, -q_2)h_2(x_2, -q'_2)\langle F_1^*(q_1)F_1(q'_1)F_2^*(q_2)F_2(q'_2) \rangle dq_1 dq'_1 dq_2 dq'_2, \quad (3)$$

*Corresponding author: wangkg@bnu.edu.cn

where $h_i(x, q) = (1/\sqrt{2\pi}) \int h_i(x, x') \exp(-iqx') dx'$. Substituting Eqs. (1) and (2) into Eq. (3), we obtain the joint-intensity

$$\langle I_1(x_1)I_2(x_2) \rangle \propto \int S(q)|h_1(x_1, -q)|^2 dq \int S(q)|h_2(x_2, -q)|^2 dq + \left| \int S(q)h_1^*(x_1, -q)h_2(x_2, -q) dq \right|^2, \quad (4a)$$

$$\langle I_1(x_1)I_2(x_2) \rangle \propto \left| \int W(q)h_1(x_1, -q)h_2(x_2, q) dq \right|^2, \quad (4b)$$

for classical and quantum sources, respectively. Equations (4) show macroscopically the difference between classical and quantum coincidence imaging. For the thermal source, the first term of Eq. (4a) brings a background while the second term devotes to the coincidence imaging. Therefore, classical coincidence imaging has lower visibility than quantum one. Furthermore, the nature of the wavevectors correlations for classical and quantum sources is also reflected in the correlations of the two impulse response functions. This will cause the different imaging laws.

Now we discuss the two schemes of coincidence imaging as shown in Fig. 1. For simplicity, we assume that the beamsplitter is close to the source, so that the beam is divided immediately from the source [11]. For scheme I, the two impulse response functions are written as

$$h_1(x_1, q) = (1/\sqrt{2\pi}) \exp[ikz_1 - iqx_1 - i\frac{q^2 z_1}{2k}], \quad (5a)$$

$$h_2(x_2, q) = \frac{1}{2\pi} \sqrt{\frac{kf}{i(f-z_3)f_c}} \exp[ik(z_2 + z_3 + 2f_c) - i\frac{q^2}{2k}(z_2 + \frac{z_3 f}{f-z_3})] \\ \times \int T(x) \exp[i\frac{kx^2}{2(z_3-f)} - i(\frac{kx_2}{f_c} + \frac{qf}{f-z_3})x] dx, \quad (5b)$$

where f and f_c are the focal lengths of the imaging lens F and the collective lens F_c , respectively. z_1 and z_2 are the distances from the source to detector D_1 and lens F, respectively; z_3 is the distance between object T and lens F. $T(x)$ is the transmission function of object T. For scheme II, however, the two impulse response functions are written as

$$h_1(x_1, q) = \frac{1}{2\pi} \sqrt{\frac{k}{if_c}} \exp[ik(z_1 + 2f_c) - i\frac{z_1 q^2}{2k}] \int T(x) \exp[-i(\frac{kx_1}{f_c} + q)x] dx, \quad (6a)$$

$$h_2(x_2, q) = \sqrt{\frac{f}{2\pi(f-z_3)}} \exp[ik(z_2 + z_3) - i\frac{q^2}{2k}(z_2 + \frac{z_3 f}{f-z_3}) - i\frac{qx_2 f}{f-z_3} - i\frac{kx_2^2}{2(f-z_3)}], \quad (6b)$$

where z_1 and z_2 are the distances from the source to object T and the imaging lens F, respectively; z_3 is the distance between lens F and detector D_2 . In the broadband limit, $W(q)$ and $S(q)$ can be seen as a constant in the integration, we calculate the joint-intensity by using Eq. (4). For both the schemes, we introduce the coincidence imaging equations

$$\frac{1}{z_2 - z_1} + \frac{1}{z_3} = \frac{1}{f}, \quad \text{for classical coincidence imaging,} \quad (7a)$$

$$\frac{1}{z_2 + z_1} + \frac{1}{z_3} = \frac{1}{f}, \quad \text{for quantum coincidence imaging,} \quad (7b)$$

under which the coincidence imaging is obtained to be

$$\langle I_1(x_1)I_2(x_2) \rangle \sim \begin{cases} |T[x_1(f-z_3)/f]|^2, & \text{for scheme I,} \\ |T[x_2 f/(f-z_3)]|^2, & \text{for scheme II.} \end{cases} \quad (8)$$

Note that Eq. (8) is valid for both quantum and classical cases when the background term is removed for the classical case. The coincidence imaging (8) is independent of position x_2 (x_1) of detector D_2 (D_1) for scheme I (II), since detector D_2 (D_1) and lens F_c form a collective detection. However, z_3 is the object distance for scheme I or the imaging distance for scheme II, so that Eq. (8) gives the same magnification as that in ordinary imaging.

In the coincidence imaging equation (7), the joint-path $z_2 \pm z_1$ is the imaging distance for scheme I or the object distance for scheme II, reflecting the nature of the quantum and classical correlations. Though the coincidence imaging equation is similar to the ordinary one, it will cause rich and even surprising imaging effects that cannot be covered

by the ordinary imaging law, for example, a virtual image can become real, and vice versa. Let us discuss two schemes in details.

Scheme I: When the object distance is greater than the focal length $z_3 > f$, the joint-path $z_2 \pm z_1$ as the image distance is positive. But this does not assure a real coincidence image. Since z_2 is positive due to definiteness, and z_1 could be either positive or negative: the former causes a real coincidence image while the latter causes a virtual one. In the case $z_3 > f$, the condition for a real coincidence imaging is $(z_3 - f)/(z_3 f) - z_2 > 0$ (< 0) for the source with quantum entanglement (classical thermal correlation). Under the opposite condition, however, the coincidence image is virtual. A virtual coincidence image can not be directly observed in the coincidence detection.

Then we consider the case of the object distance less than the focal length $z_3 < f$, for which the joint-path $z_2 \pm z_1$ as the image distance is negative. This derives that z_1 is negative for the quantum coincidence imaging and positive for the classical coincidence imaging. Therefore, a virtual image in the ordinary imaging system becomes real in the classical coincidence imaging.

The coincidence imaging can be plotted by the graphics of the ray optics, by taking into account the correlation of rays emitted from the source. In graphics, we first plot the image by the ordinary way. Then, for the source with quantum entanglement, the image is reflected twice, first by the source and then by the beamsplitter. Obviously, the beamsplitter plays the role as a mirror. However, the quantum source emits a pair of correlated rays with the opposite transverse wavevectors, one to object and the other to image, so that it also acts as a mirror. For the source with the thermal correlation, the image is reflected only by the beamsplitter. This geometry is due to the nature of the self-correlation of the wavevectors, so that the thermal source acts as a phase-conjugate mirror and hence the image is reflected to itself. According to these rules, we plot the coincidence imaging for $z_3 > f$ in Figs. 2 and 3, and $z_3 < f$ in Fig. 4. For comparison, we arrange the same optical setup for the two sources: the quantum entanglement in Figs. 2a-4a and the classical thermal correlation in Figs 2b-4b. These figures verify the above analysis: while the quantum coincidence image is virtual, the classical coincidence image must be real, or vice versa.

Scheme II: In this scheme, the joint-path $z_2 \pm z_1$ is the object distance while z_3 is the image distance. Just as the ordinary imaging law, when the joint-path $z_2 \pm z_1$ is greater (less) than the focal length, the coincidence image is real (virtual). Different from scheme I, for the same optical setup with different sources, the quantum and classical coincidence images can be both real. In Fig. 5, we plot the two real coincidence images for $z_2 \pm z_1 > f$. In the graphics of this scheme, we should move the object to the optical axes of the lens. For the source with the quantum entanglement, the object is reflected twice, first by the beamsplitter and then by the source, as shown in Fig. 5a. For the classical correlation, however, the object is reflected only by the beamsplitter, as shown in Fig. 5b.

The spatial thermal correlation (1) exists in the SPDC process. In type II SPDC, the quantum entanglement occurs between two beams with different polarizations. But if one beam with a particular polarization is extracted, it has the thermal correlation [10]. However, the beam generated in type I SPDC may incorporate both the quantum entanglement and the classical thermal correlation [10]. When the gain of SPDC is lower, the power of the thermal correlation is lower than that of the quantum entanglement, i.e. $|S(q)| < |W(q)|$. In the strong coupling of SPDC, $|S(q)|$ is increased and comparable with $|W(q)|$ [9]. Using this source, it can form a dual coincidence imaging system, in which two kinds of coincidence imaging are created simultaneously. For scheme I, classical coincidence image is real while quantum one must be virtual, and vice versa. For scheme II, however, two images can be both real, or both virtual, or one is real and the other virtual, depending on the values of z_1 and z_2 .

In summary, we show the macroscopic difference of quantum and classical coincidence imaging. The unusual and rich coincidence imaging effects may provide potential application in novel optical designs.

The authors thank L. A. Wu for helpful discussions. This research was supported by the National Fundamental Research Program of China with No. 2001CB309310, and the National Natural Science Foundation of China, Project Nos. 60278021 and 10074008.

-
- [1] D. V. Strekalov, A. V. Sergienko, D. N. Klyshko, and Y. H. Shih, Phys. Rev. Lett. **74**, 3600 (1995); T. B. Pittman, Y. H. Shih, D. V. Strekalov, and A. V. Sergienko, Phys. Rev. A **52**, R3429 (1995).
 - [2] P. H. S. Ribeiro, S. Pádua, J. C. Machado da Silva, and G. A. Barbosa, Phys. Rev. A **49**, 4176 (1994).
 - [3] B. E. A. Saleh, A. F. Abouraddy, A. V. Sergienko, and M. C. Teich, Phys. Rev. A **62**, 043816 (2000).
 - [4] A. F. Abouraddy, B. E. A. Saleh, A. V. Sergienko, and M. C. Teich, Phys. Rev. Lett. **87**,123602 (2001); J. Opt. Soc. Am. B **19**, 1174 (2002).
 - [5] A. Gatti, E. Brambilla, and L. A. Lugiato, Phys. Rev. Lett. **90**, 133603 (2003).

- [6] R. S. Bennink, S. J. Bentley and R. W. Boyd, Phys. Rev. Lett. **89**, 113601 (2002); R. S. Bennink, S. J. Bentley, R. W. Boyd, and J. C. Howell, Phys. Rev. Lett. **92**, 033601 (2004).
- [7] M. D'Angelo and Y. Shih, quant-ph/0302146; M. D'Angelo, Y. -H. Kim, S. P. Kulik, and Y. Shih, Phys. Rev. Lett. **92**, 233601 (2004).
- [8] A. Gatti, E. Brambilla, M. Bache and L. A. Lugiato, quant-ph/0307187.
- [9] D. Zh. Cao and K. Wang, quant-ph/0310046; D. Zh. Cao, Zh. Li, Y. H. Zhai, and K. Wang, quant-ph/0401109.
- [10] K. Wang and D. Zh. Cao, quant-ph/0404078.
- [11] The further theoretical analysis shows that this assumption is not necessary to obtain the imaging equations (7).

Captions of Figures

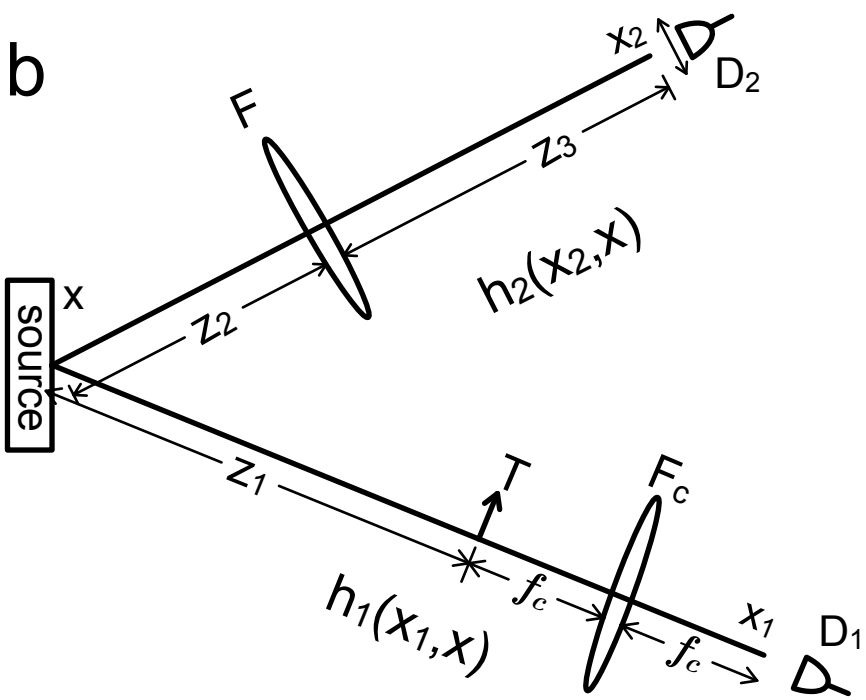
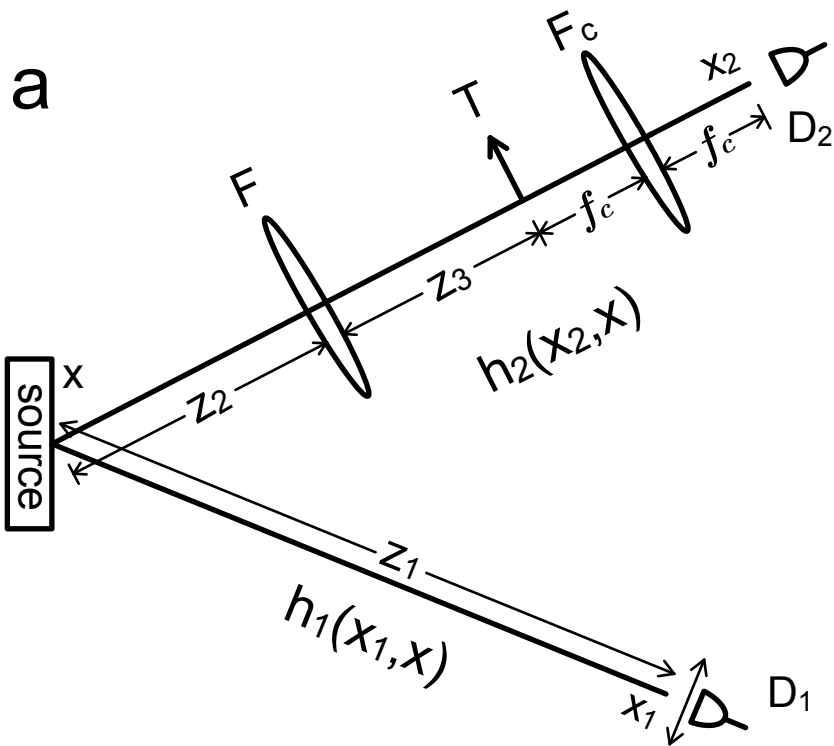
Fig. 1 The sketches of coincidence imaging for (a) scheme I, where object T and the imaging lens F are in the same path and (b) scheme II, where T and F are in the different paths. F_c is the collective lens so that the object and the detector are placed in its two focal planes.

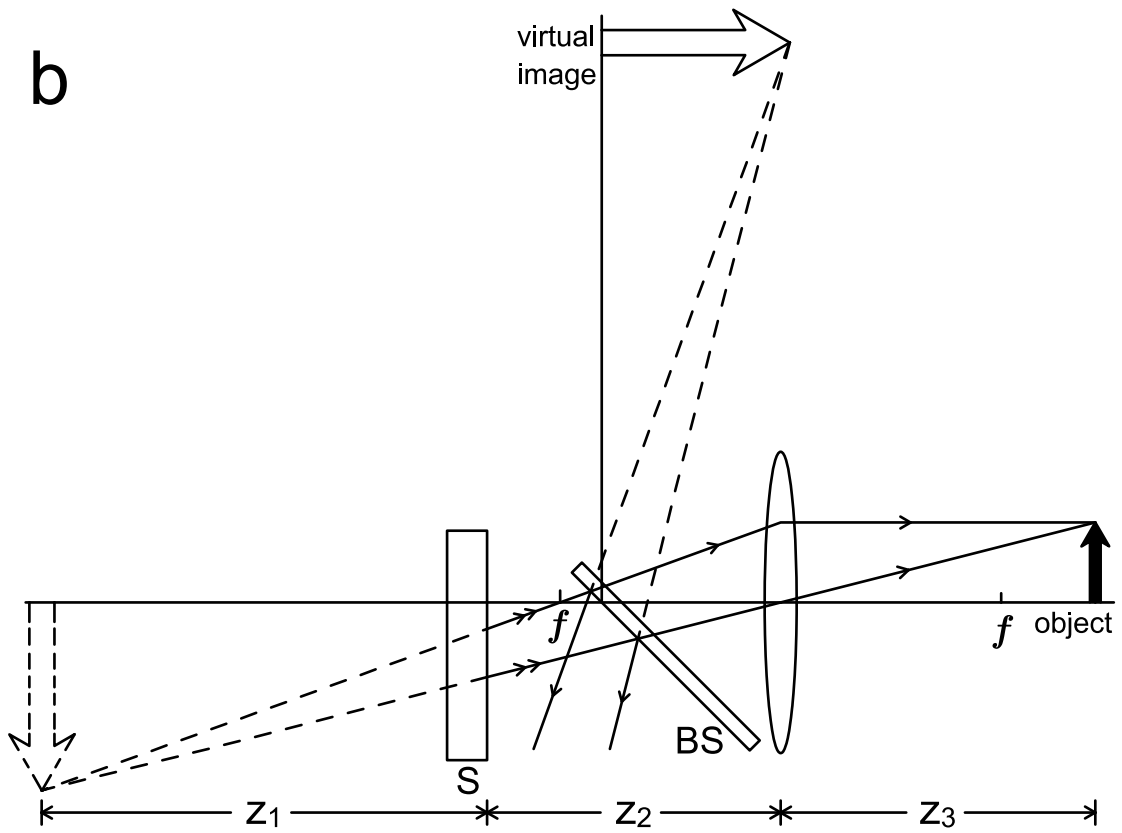
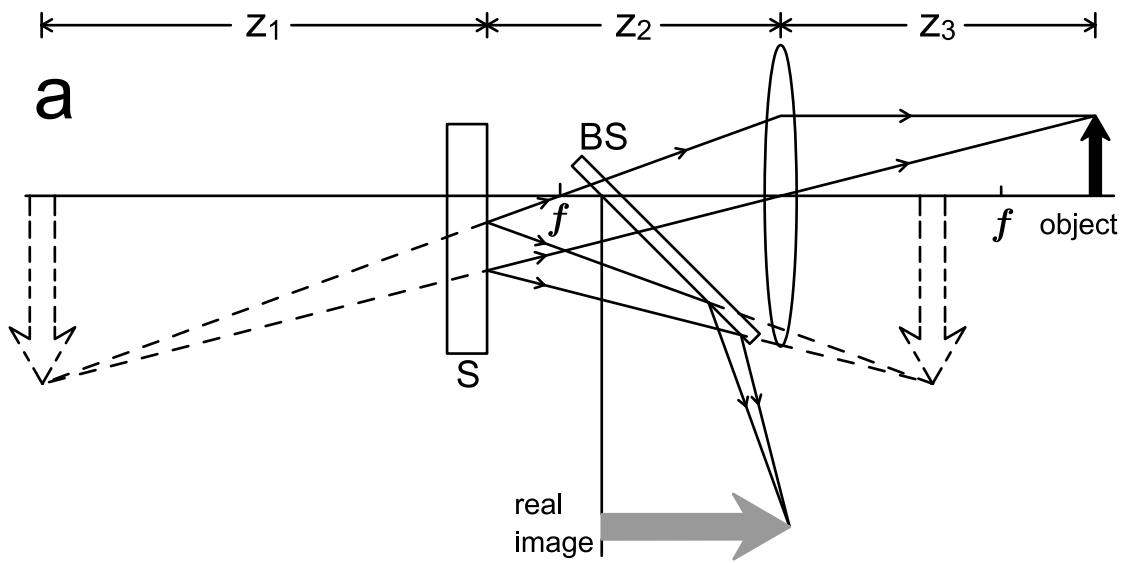
Fig. 2 Coincidence imaging for scheme I in which $z_3 > f$ and the condition $\frac{z_3-f}{z_3f} - z_2 > 0$ are satisfied. (a) a real coincidence image is formed for the source with the quantum entanglement; (b) a virtual coincidence image is formed for the source with the thermal correlation. In Figs. 2-5, the intermedial images are indicated by dashed lines.

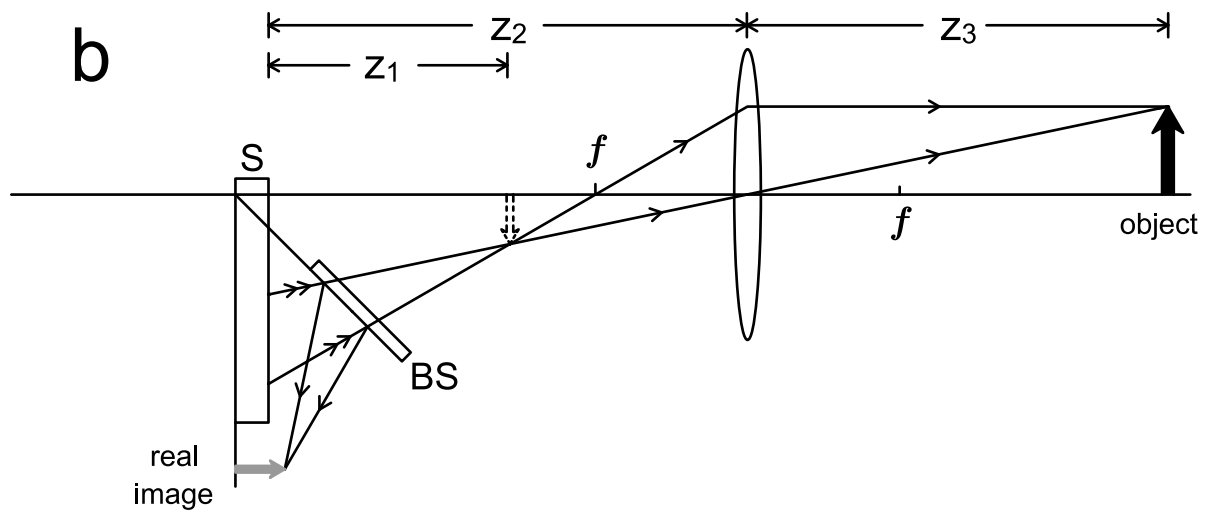
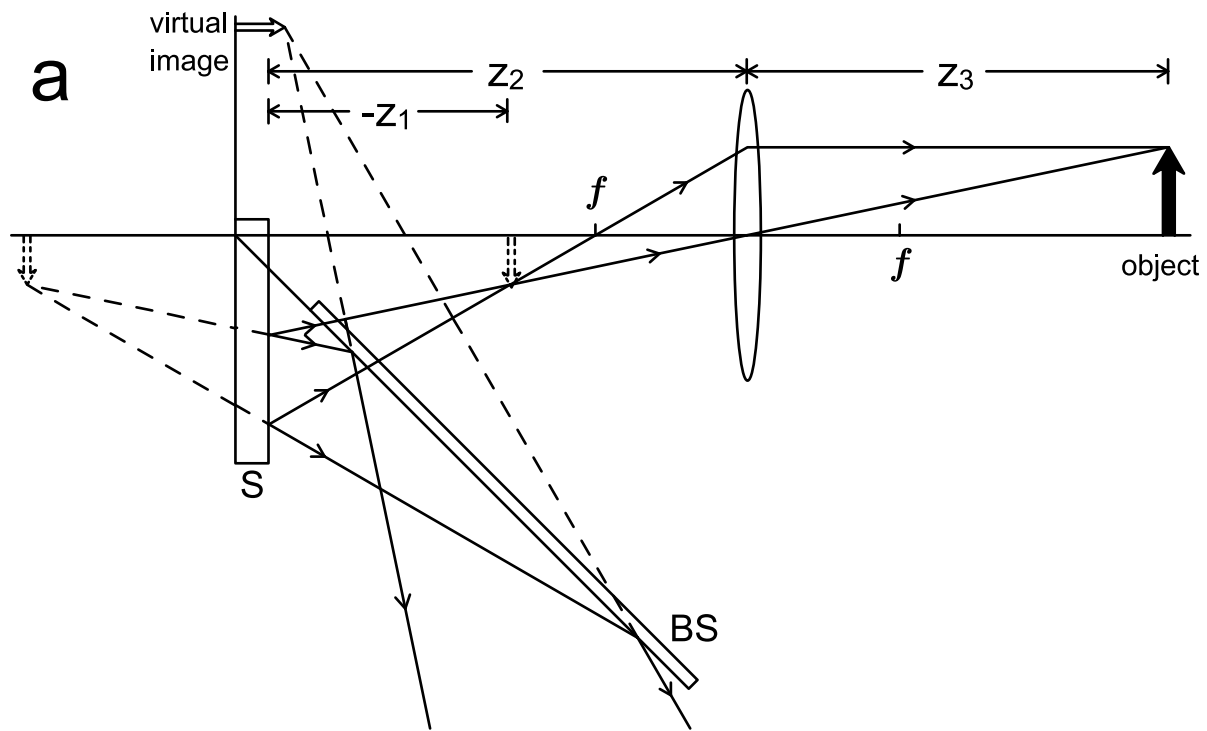
Fig. 3 Same as in Fig. 2 but the condition $\frac{z_3-f}{z_3f} - z_2 < 0$ is satisfied. (a) a virtual coincidence image is formed for the source with the quantum entanglement; (b) a real coincidence image is formed for the source with the thermal correlation.

Fig. 4 Coincidence imaging for scheme I in the case $z_3 < f$. (a) a virtual coincidence image is formed for the source with the quantum entanglement; (b) a real coincidence image is formed for the source with the thermal correlation.

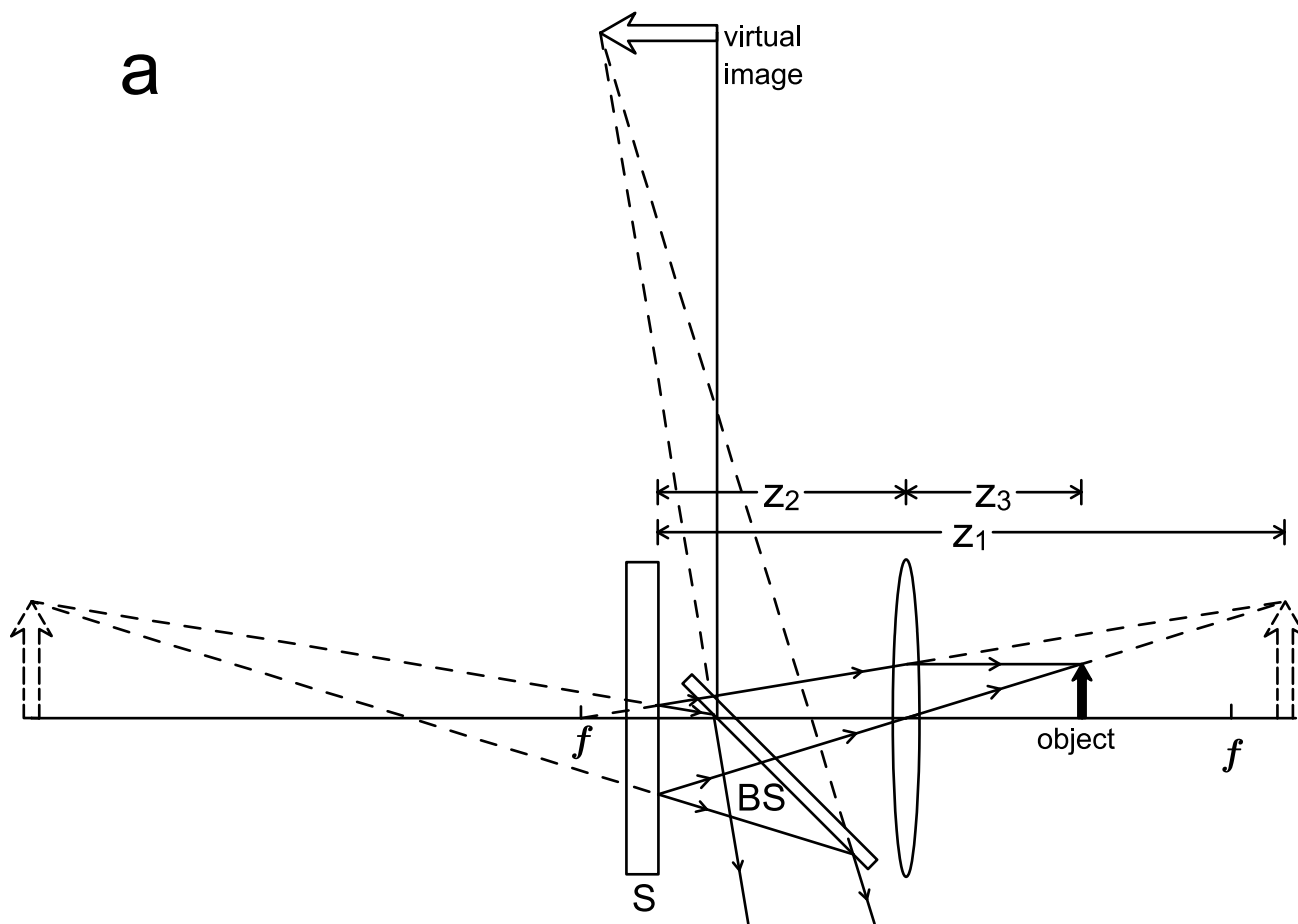
Fig. 5 Coincidence imaging for scheme II in the case $z_2 \pm z_1 > f$. The real coincidence images are formed for both the sources: (a) with the quantum entanglement and (b) with the thermal correlation.







a



b

